# Tuning the Resonance in High-Temperature Superconducting Terahertz Metamaterials

Hou-Tong Chen,[1,*] Hao Yang,[1,2] Ranjan Singh,[1] John F. O'Hara,[1] Abul K. Azad,[1] Stuart A. Trugman,[1] Q. X. Jia,[1] and Antoinette J. Taylor[1]

[1]*MPA-CINT, MS K771, Los Alamos National Laboratory, Los Alamos, New Mexico 87545, USA*

[2]*School of Physical Science and Technology, Soochow University, Suzhou 215006, China*

(Received 9 August 2010; revised manuscript received 16 November 2010; published 10 December 2010)

In this Letter, we present resonance properties in terahertz metamaterials consisting of a split-ring resonator array made from high-temperature superconducting films. By varying the temperature, we observe efficient metamaterial resonance switching and frequency tuning. The results are well reproduced by numerical simulations of metamaterial resonance using the experimentally measured complex conductivity of the superconducting film. We develop a theoretical model that explains the tuning features, which takes into account the resistive resonance damping and additional split-ring inductance contributed from both the real and imaginary parts of the temperature-dependent complex conductivity. The theoretical model further predicts more efficient resonance tuning in metamaterials consisting of a thinner superconducting split-ring resonator array, which are also verified in subsequent experiments.

DOI: 10.1103/PhysRevLett.105.247402 PACS numbers: 78.67.Pt, 74.25.−q, 74.78.−w

Metamaterials consisting of metallic elements have enabled a structurally scalable electrical and/or magnetic resonant response, from which exotic electromagnetic phenomena absent in natural materials have been observed [1]. Metals provide high conductivity that is necessary to realize strong electrical and magnetic metamaterial response [2,3]. Metals, however, play a negligible role in active and dynamical metamaterial resonance switching and/or frequency tuning, which has been typically accomplished through the application of external stimuli [4–12] when other natural materials (e.g., semiconductors) or devices are integrated into metamaterials. It is essentially the modification of the metamaterial embedded environment that contributes to such previously observed functionalities.

Recently, there has been increasing interest in superconducting metamaterials due to the facts below: (i) Layered superconductors could realize negative refractive index metamaterials [13,14]; (ii) superconducting quantum interference devices could be integrated [15,16]; (iii) diamagnetic metamaterial response was achieved at very low frequencies [17,18]; (iv) high conductivity towards loss reduction [19–21]; and (v) resonance tuning [20–26]. At low temperatures, superconducting materials possess superior conductivity than metals at frequencies up to terahertz (THz), and therefore it is expected that superconducting metamaterials will have a lower loss than metal metamaterials. More interestingly, superconductors exhibit tunable complex conductivity over a wide range of values, through variation of temperature and application of photoexcitation and electrical and magnetic fields. Therefore, we would expect correspondingly tunable metamaterials, which originate from the superconducting materials composing the metamaterial, in contrast to tuning the metamaterial environment.

At THz frequencies, high-temperature superconductors should be employed, in which THz radiation would not easily break Cooper pairs. In this Letter, we present THz metamaterials based on electric split-ring resonators (SRRs) made from epitaxial $YBa_2Cu_3O_{7-\delta}$ (YBCO) high-temperature superconducting films with $\delta = 0.05$, which were prepared by using pulsed laser deposition on 500 $\mu$m thick (100) $LaAlO_3$ (LAO) substrates. The transition temperature was measured to be $T_c = 90$ K. Square arrays of electric SRRs, with the dimensions specified in the unit cell microscopic image shown in the inset in Fig. 1(a), were fabricated by using conventional photolithographic methods and wet chemical etching of the YBCO films with thicknesses of $d = 180$ or 50 nm. THz time-domain spectroscopy incorporated with a continuous flow liquid helium cryostat was used to characterize the YBCO films and metamaterials. Under normal incidence, the THz transmission spectra were measured as a function of temperature, by using an LAO substrate as the reference. These metamaterials exhibit interesting temperature-dependent resonance strength and frequency. Finite-element numerical simulations and theoretical modeling were performed to understand the underlying tuning mechanism.

We focus our attention on the metamaterial fundamental resonance (the so-called $LC$ resonance) resulting from the circulating currents excited by the incident THz electric field [27]. In Fig. 1(a), we show the THz transmission amplitude spectra for the 180 nm thick YBCO metamaterial sample at various temperatures. At temperatures far below $T_c$, e.g., 20 K, the metamaterial exhibits the strongest resonance, as indicated by the sharp THz transmission dip with a minimal transmission amplitude of 0.05 at 0.61 THz. This strong resonance is almost the same as in a metamaterial sample where the YBCO SRRs were replaced by gold SRRs with the same thickness and at the

 

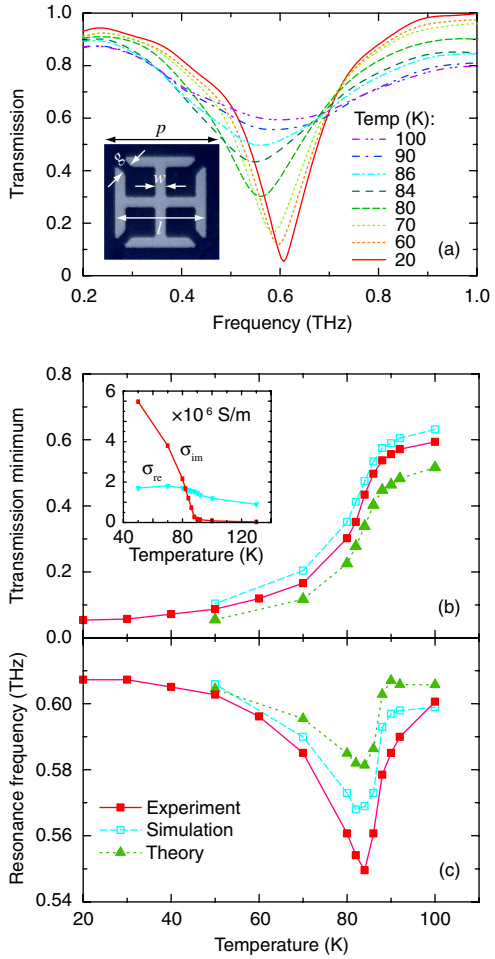


FIG. 1 (color online). (a) THz transmission amplitude spectra of the 180 nm thick YBCO metamaterial at various temperatures. (b) Transmission minimum and (c) corresponding resonance frequency as functions of temperature, from experiments, numerical simulations, and theoretical calculations. The inset in (a) illustrates a microscopic image of a single YBCO SRR, where the lighter colored area is YBCO, $l = 36\ \mu$m, $w = 4\ \mu$m, $g = 4\ \mu$m, and $p = 46\ \mu$m. The inset in (b) shows the real and imaginary parts of the complex conductivity at 0.6 THz of an unpatterned 180 nm thick YBCO film.

same temperature. As the temperature increases, the resonance strength decreases, as seen by the broadening and reduction in amplitude of the transmission dip. The resonance frequency experiences a redshifting, which reaches the lowest value of 0.55 THz near 84 K, resulting in a frequency tuning of 10%. As the temperature further increases, the resonance strength continues to decrease, but the resonance frequency, on the other hand, shifts back to higher frequencies. The temperature-dependent transmission minimum and resonance frequency are plotted in Figs. 1(b) and 1(c), respectively. The results show that, at temperatures near 84 K, the transition of resonance strength is fastest and the resonance frequency exhibits a dip, not observed in previous work [20,24–26]. Similar features of the resonance tuning were also observed in all of the several other YBCO metamaterial samples with approximately the same thickness. We can exclude the LAO substrate as contributing to the metamaterial resonance tuning, because the features in the temperature-dependent resonance in the YBCO metamaterials (see Fig. 1) were not observed in a metamaterial sample where the YBCO was replaced by gold. Therefore, it is the temperature-dependent properties of YBCO film that are responsible for the observed metamaterial resonance tuning.

The complex conductivity of YBCO film can be expressed by using the well-known two-fluid model [28]:

$$\sigma_{\mathrm{re}} = \frac{ne^2}{m^*}\frac{f_n(T)\tau}{1+\omega^2\tau^2}, \tag{1}$$

$$\sigma_{\mathrm{im}} = \frac{ne^2}{m^*}\left[\frac{f_n(T)\omega\tau^2}{1+\omega^2\tau^2} + \frac{f_s(T)}{\omega}\right], \tag{2}$$

where $f_n$ and $f_s$ are fractions of normal (quasiparticle) and superconducting (superfluid) carriers, respectively, with $f_n + f_s = 1$, $n$ is the carrier density, $m^*$ is the carrier effective mass, and $\tau$ is the quasiparticle relaxation time. Using THz time-domain spectroscopy we experimentally measured the conductivity of an unpatterned 180 nm thick YBCO plain film. The resultant real and imaginary parts of the complex conductivity at 0.6 THz are plotted as functions of temperature in the inset in Fig. 1(b). The real conductivity [Eq. (1)], which derives from the Drude response of quasiparticles, slowly increases when the temperature decreases across $T_c$ to about 70 K. It starts to decrease below 70 K, but not significantly, over the temperatures we measured down to 50 K. In this temperature range, $\omega\tau \ll 1$ at the resonance frequency ( $\sim 0.6$ THz), the decreasing $f_n(T)$ may be compensated by the increasing quasiparticle scattering time $\tau$ [29]. At temperatures above $T_c$, the imaginary conductivity is derived from the Drude response and is very small, since $f_s(T > T_c) = 0$. As the temperature decreases below $T_c$, the second term in Eq. (2) from the superfluid Cooper pair state becomes nonzero and results in the rapidly increasing imaginary conductivity, exceeding the real conductivity below 82 K. By using these experimental values of the YBCO complex conductivity at 0.6 THz, the metamaterial resonant response was simulated with commercially available finite-element simulation codes from COMSOL Multiphysics. The simulated transmission minimum and the corresponding frequency are plotted as functions of temperature in Figs. 1(b) and 1(c), respectively, reproducing the resonance tuning features observed in experiments.

The relatively small variation of real conductivity cannot solely cause the observed large metamaterial resonance switching and frequency tuning. Both the real and imaginary parts of the complex conductivity have to be considered for the metamaterial resonance. The imaginary conductivity becomes dominant at low temperatures, and it is responsible for the enhancement in resonance strength. The resonance frequency is determined by the effective capacitance $C$, inductance $L$, and resistance $R$ in the SRRs [30]:

$$\omega_0^2 = \frac{1}{LC} - \frac{R^2}{4L^2}. \quad (3)$$

It has been shown that the kinetic inductance plays an important role in determining the metamaterial resonance frequency [20,31]. This effect underpins the redshifting of the resonance frequency (0.6%) in niobium metal superconducting metamaterials operating near 10 GHz as the temperature increases and approaches $T_c$ [20]. However, the back blueshifting, shown in Fig. 1(c) between ~84 K and $T_c$, was not observed in niobium, and the model proposed in that work would not explain this effect when only the superfluid state (i.e., imaginary conductivity) was considered [20].

Here we consider a more general situation where the SRRs are fabricated from a conducting film (YBCO film in our case) with a complex conductivity $\tilde{\sigma}$ and thickness $d$. Such an unpatterned plain film can be modeled as a lumped impedance in an equivalent transmission line model. By equating the (multiple) reflections or transmissions from the film and the transmission line model, this complex surface impedance (or sheet impedance with units of $\Omega$/square) of the unpatterned film can be derived as

$$\tilde{Z}_S = R_S - iX_S = Z_0 \frac{n_3 + i\tilde{n}_2 \cot(\tilde{\beta}d)}{\tilde{n}_2^2 - n_3^2} \cong i\frac{Z_0}{\tilde{n}_2}\cot(\tilde{\beta}d), \quad (4)$$

where the tildes over the variables indicate complex values, $Z_0 = 377\ \Omega$ is the vacuum intrinsic impedance, $n_3 = \sqrt{\epsilon_{\mathrm{LAO}}} = 4.8$ is the LAO substrate refractive index, $\tilde{n}_2 = \sqrt{i\tilde{\sigma}/\epsilon_0\omega}$ is the complex refractive index of the film, and $\tilde{\beta} = \tilde{n}_2\omega/c_0$ is the complex propagation constant where $c_0$ is the light velocity in vacuum. Both $\tilde{n}_2$ and $\tilde{\beta}$ can be calculated from the experimental complex conductivity near the metamaterial resonance frequency, where $n_3 \ll |\tilde{n}_2|$ results in the final simplification in Eq. (4). It becomes obvious that both the finite real and imaginary parts of $\tilde{n}_2$, and therefore $\tilde{\sigma}$, contribute to the film surface resistance $R_S$ and reactance $X_S$. They are plotted in Fig. 2 for the 180 nm thick YBCO film as functions of temperature and are also calculated for a 50 nm thick YBCO film assuming its complex conductivity does not depend on the film thickness.

The YBCO SRR array resistance $R$ (SRR reactance $X$ is zero at resonance) can be obtained by considering the nonuniform distribution of currents in a unit cell [32]: $R \cong [(A-g)/w]R_S$, where $A = 64\ \mu$m is the median circumference of the (small) current loop. When the temperature increases, the increasing SRR resistance $R$ accounts for the resonance damping and therefore the increasing transmission minimum. If we model the SRR array as a lumped resistor $R$ in the transmission line [33], we can calculate the resonance transmission as a function of temperature, which is plotted in Fig. 1(b) and satisfyingly reproduces the experimental and simulated results.

In order to correctly interpret the temperature-dependent resonance frequency shifting, additional inductance in SRRs has to be taken into account besides the geometric

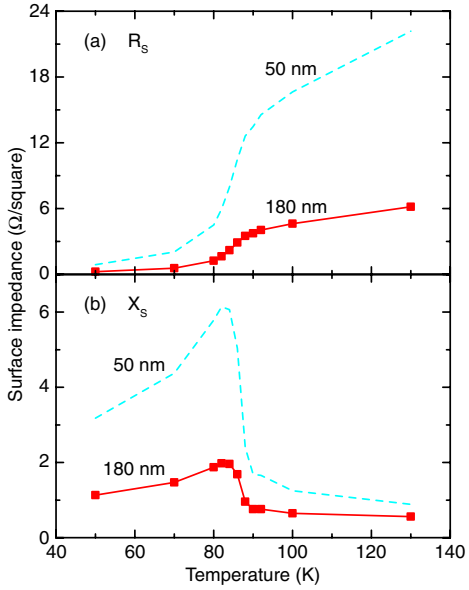


FIG. 2 (color online). Complex surface impedance of the 180 nm thick unpatterned YBCO superconducting film calculated by using the experimental complex conductivity at 0.6 THz. (a) Surface resistance $R_S$, and (b) surface reactance $X_S$. The dashed curves are for an assumed 50 nm thick YBCO film.

inductance $L_G$. The geometric inductance represents the conventional inductance of the SRR loop and can be estimated [34] to be $L_G \cong 4 \times 10^{-11}$ H. The additional SRR inductance $L_S$ can be calculated by using the above derived YBCO film surface reactance $X_S$ and by considering the geometry and dimensions of the YBCO SRR: $L_S \cong [(A-g)/w](X_S/\omega)$. Therefore, the total SRR inductance becomes $L = L_G + L_S$. In order to obtain the metamaterial resonance frequency by using Eq. (3), we estimate the SRR capacitance $C \cong 1.5 \times 10^{-15}$ F, from the above estimated geometric inductance $L_G$ and the simulated resonance frequency $\omega_0 = 2\pi \times 0.62$ THz assuming perfect conducting SRRs (i.e., $L_S = 0$ and $R = 0$). The calculated temperature-dependent metamaterial resonance frequency is plotted in Fig. 1(c) along with the experimental and simulation results. Again, the theoretical result reproduces the frequency tuning features, though the calculated and simulated frequency tuning range is smaller than the experimental data. The apparent discrepancy in frequency tuning range could arise from (i) the accuracy of conductivity measurements and its variation among samples; (ii) the values of the frequency-dependent conductivity were taken at 0.6 THz for all temperatures in numerical simulations and theoretical calculations, while the resonance frequency is a function of temperature; (iii) in theoretical calculations we neglected the coupling among the small loops within the SRR unit cell; and (iv) the fabrication tolerance of the YBCO metamaterial samples.

Equation (4) further reveals that, for a fixed value of the real conductivity, which is approximately the case in our situation, the YBCO film surface reactance, and therefore the additional SRR inductance, reaches the maximum

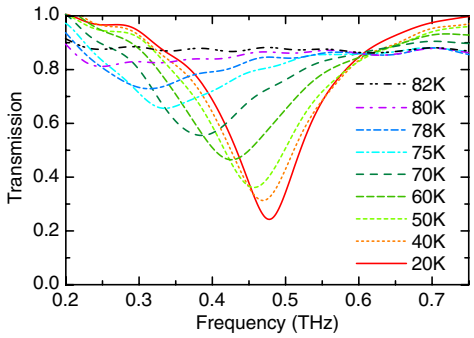


FIG. 3 (color online). Temperature-dependent THz transmission amplitude spectra of the 50 nm thick YBCO metamaterial.

value when the imaginary conductivity is approximately equal to the real conductivity, and vice versa. This is consistent with the experimental observations, where the metamaterial resonance frequency shifts to the lowest value when the real and imaginary parts of the YBCO complex conductivity cross each other.

The results in Fig. 2 suggest that metamaterials made from thinner YBCO superconducting films will have a lower resonance frequency and will be more efficient in resonance switching and frequency tuning. This is verified by subsequent experiments using a second metamaterial sample fabricated from 50 nm thick YBCO film. The temperature-dependent transmission spectra are shown in Fig. 3. The resonance frequency at 20 K is measured to be 0.48 THz, which is significantly lower than that in the metamaterial sample from 180 nm thick YBCO film. When the temperature increases, the resonance frequency continuously shifts to lower frequencies. It becomes 0.31 THz at 78 K, achieving a tuning range of 35%. We did not observe the back blueshifting of resonance frequency due to the high resistive damping in this thinner YBCO metamaterial sample at temperatures above 80 K.

In conclusion, we have fabricated and characterized electric SRR-based metamaterials from high-temperature superconducting YBCO films. We observed temperature-induced metamaterial resonance switching and frequency tuning, which can be reproduced by finite-element numerical simulations using the experimentally measured complex conductivity of the YBCO film. We found that both the temperature-dependent real and imaginary parts of the complex conductivity of the superconducting film have to be consistently considered in order to achieve a correct interpretation. A theoretical model has been developed, taking into account the SRR resistance and additional inductance. Our modeling calculations were in reasonably good agreement with experimental observations and numerical simulations and further predicted more efficient resonance switching and frequency tuning with thinner YBCO metamaterials, which was also verified in subsequent experiments. We expect that such resonance tuning in superconducting metamaterials could also be realized dynamically through application of optical excitation, electrical, and magnetic fields. Although high-temperature superconducting metamaterials may not be able to essentially address the loss issue at THz frequencies and beyond, they should enable the development of novel, multifunctional metamaterials.

We acknowledge support from the Los Alamos National Laboratory LDRD Program and the Center for Integrated Nanotechnologies.

*chenht@lanl.gov

[1] D. R. Smith *et al.*, Phys. Rev. Lett. **84**, 4184 (2000).
[2] J. B. Pendry, A. J. Holden, W. J. Stewart, and I. Youngs, Phys. Rev. Lett. **76**, 4773 (1996).
[3] J. B. Pendry, A. J. Holden, D. J. Robbins, and W. J. Stewart, IEEE Trans. Microwave Theory Tech. **47**, 2075 (1999).
[4] I. V. Shadrivov, S. K. Morrison, and Y. S. Kivshar, Opt. Express **14**, 9344 (2006).
[5] W. J. Padilla *et al.*, Phys. Rev. Lett. **96**, 107401 (2006).
[6] H.-T. Chen *et al.*, Nature (London) **444**, 597 (2006).
[7] E. Kim *et al.*, Appl. Phys. Lett. **91**, 173105 (2007).
[8] H.-T. Chen *et al.*, Nat. Photon. **2**, 295 (2008).
[9] H.-T. Chen *et al.*, Nat. Photon. **3**, 148 (2009).
[10] T. Driscoll *et al.*, Science **325**, 1518 (2009).
[11] H. Tao *et al.*, Phys. Rev. Lett. **103**, 147401 (2009).
[12] K. M. Dani *et al.*, Nano Lett. **9**, 3565 (2009).
[13] A. Pimenov, A. Loidl, P. Przyslupski, and B. Dabrowski, Phys. Rev. Lett. **95**, 247009 (2005).
[14] A. L. Rakhmanov *et al.*, Phys. Rev. B **81**, 075101 (2010).
[15] C. Du, H. Chen, and S. Li, Phys. Rev. B **74**, 113105 (2006).
[16] N. Lazarides and G. P. Tsironis, Appl. Phys. Lett. **90**, 163501 (2007).
[17] B. Wood and J. B. Pendry, J. Phys. Condens. Matter **19**, 076208 (2007).
[18] F. Magnus *et al.*, Nature Mater. **7**, 295 (2008).
[19] M. Ricci, N. Orloff, and S. M. Anlage, Appl. Phys. Lett. **87**, 034102 (2005).
[20] M. C. Ricci and S. M. Anlage, Appl. Phys. Lett. **88**, 264102 (2006).
[21] Y. Wang and M. J. Lancaster, IEEE Trans. Appl. Supercond. **16**, 1893 (2006).
[22] H. Salehi, A. H. Majedi, and R. R. Mansour, IEEE Trans. Appl. Supercond. **15**, 996 (2005).
[23] M. C. Ricci *et al.*, IEEE Trans. Appl. Supercond. **17**, 918 (2007).
[24] V. A. Fedotov *et al.*, Opt. Express **18**, 9015 (2010).
[25] J. Gu *et al.*, Appl. Phys. Lett. **97**, 071102 (2010).
[26] B. Jin *et al.*, Opt. Express **18**, 17 504 (2010).
[27] H.-T. Chen *et al.*, Opt. Express **15**, 1084 (2007).
[28] M. Tinkham, *Introduction to Superconductivity* (McGraw-Hill, New York, 1996), 2nd ed.
[29] F. Gao *et al.*, Phys. Rev. B **54**, 700 (1996).
[30] E. M. Purcell, *Electricity and Magnetism* (McGraw-Hill, New York, 1985), 2nd ed.
[31] J. Zhou *et al.*, Phys. Rev. Lett. **95**, 223902 (2005).
[32] R. Ulrich, Infrared Phys. **7**, 37 (1967).
[33] J. F. O'Hara *et al.*, Act. Passive Electron. Compon. **2007**, 1 (2007).
[34] F. E. Terman, *Radio Engineers' Handbook* (McGraw-Hill, New York, 1943).